Synthesis of Green Inhibitor for Mild Steel Corrosion in a Sulphuric Acid Medium

Ompal Singh Yadav*, Reshu Chaudhary and Ashu Gupta

Shyamlal College Shahdara, Delhi-110032, India
Corresponding author: opduchem@gmail.com

Received 30/03/2023; accepted 05/06/2023
https://doi.org/10.4152/pea.2024420504

Abstract
MS corrosion behavior was herein studied via green azo methane, i.e., BDTT, in a 0.5 M H_2SO_4 solution. CI mechanisms were investigated by Ec techniques (PDP, EIS and WL). Experimental studies results were supplemented with theoretical calculations, DFT and various Td adsorption and activation parameters. BDTT molecule mechanism of adsorption onto the MS surface followed Langmuir's isotherm. In this study, an eco-friendly and cost-effective strategy to hinder corrosion was proposed.

Keywords: BDTT; CI; DFT; EIS; PDP; WL.

Introduction•

Metals and its alloy are materials of wide application in construction and industry. Generally, acidic solutions are good cleaners, being used for many purposes. However, due to acids corrosive nature, the materials (metals) exposed to them suffer serious degradation that causes high losses and costs. The most challenging challenge faced by researchers and industrialists is metallic corrosion prevention and control. Acidic media destructive effects on the environment are metals dissolution and Ec reactions. Corrosion risks are reduced by several organic inhibitors that have donor sites, with existing heteroatoms such as N, S and O, unsaturated π-bonds and aromatic ring conjugation with planarity, which are considered as effectively adsorption sites, due to their available lone pair of electrons [1-6]. Nowadays, CI based on heavy metals have been restricted in numerous countries, due to their hazardous effect upon nature and humans. Dichromates and chromates originated CI are fairly better IE(%). However, due to their toxic nature, they pose a high risk for human health and the eco-system [7]. Thus, [8-10] selected organic molecules rather than inorganic ones, since they are nontoxic and environment friendly. Organic compounds IE(%) in acidic solutions depends on their interaction with metal surfaces. Stronger interactions with metals surfaces increase organic CI compounds adsorption properties, enhancing their IE(%). CI are adsorbed onto metal surfaces either chemically, physically or both [11]. Schiff base (azo methine) compounds, which contain N and S atoms, were also investigated [12-18]. Generally, Schiff bases credit is growing in materials

• The abbreviations and symbol definition lists are in pages 368-369.

science, since their starting materials are strong, their synthesis route is relatively easy, they have low toxicity, and are very ecofriendly [19-21].
The aim of this study was to produce a CI, through a synthetized Schiff base compound (E)-5- (benzylideneamino)-1,3,4 thiadiazole-2-thiol (green azo methane). BDTT was used as CI on WE (MS) in a 0.5 M H_2SO_4 solution. Investigations were done with or without BDTT, in various Ct, by Ec techniques (PDP, LPR and EIS) and WL methods. Quantum chemical parameters with optimized molecular structure were calculated via DFT method.

Materials and methods

BDTT synthesis

BDTT was synthesized through the addition reaction method, [22] which consists in having $C_2H_3N_3$ to react with C_7H_6O. $C_2H_3N_3$ (6.21 mM) solution was prepared by dissolving it in absolute C_2H_6O (100 mL), in a round bottom flask. C_7H_6O (0.49 mM) was dissolved in dry C_2H_6O, in another 100 mL beaker. Then, C_7H_6O solution was drop wise added to $C_2H_3N_3$ mixture, in a 250 mL round bottom flask. Further reaction mixtures were constantly refluxed for 10 h, through continuous stirring. The reaction was monitored by TLC, at regular intervals. Finally, the precipitate was obtained by filtration, and thoroughly washed with ether. The resulting compound was a light yellow colored solid, with good yields.

CI studies via gravimetric technique

WE formation

MS cuboidal coupons, with the dimensions of 1 × 1 × 1 cm and 4 × 1 × 1 cm, were used for WL and Ec methods, respectively. MS coupons composition was 98.72 Fe, 1.02 Mn, 0.15 C, 0.08 Si and 0.02 S (%).

Test solution preparation

The employed solvents were distilled water and C_2H_6O. The reactants and solvents (AR grade) were commercially available, and used without any further purification. The electrolytes solutions for testing were prepared by AR grade concentrated H_2SO_4 dilution with double distilled water. BDTT bulk solutions with various Ct were prepared by dissolving their required amount in H_2SO_4.

WL studies

WL experiments are a simple process, in which MS was immersed in 0.5 M H_2SO_4 solutions, for 24 h, with different Ct of BDTT [23]. After 24 h, corrosion products on the MS surface were cleaned. Then, the remaining MS sample was weighed [24]. CR and IE(%) were calculated through eqs. (1) and (2). All studies were repeated more than twice, to minimize errors. WL values were further used to calculate IE(%) of BDTT against MS corrosion. The terms related to corrosion, i.e., CR and IE(%), were obtained via Eq. (1):

$$IE\% = \frac{W^a - W^i}{W^a} \times 100 \quad (1)$$

where W^a and W^i are MS coupons WL in 0.5 M H_2SO_4 solutions without and with BDTT, in various Ct.
SC (θ) by BDTT was evaluated through the following Eqs.:

$$\theta = \frac{w^a - w^i}{w^a} \quad (2)$$

$$\text{CR (mmy}^{-1}) = \frac{87.6\ X\ \Delta W}{ADt} \quad (3)$$

where ΔW is MS mass change in mg, A is MS coupon area (cm^2), t (h) is IT and D is MS density [25].

Ec measurements

The whole Ec experiment was performed with a three electrode Ec cell (250 mL). The employed electrodes were MS, Pt and SCE, as WE, CE and RE, respectively. CE and RE electrodes were fixed to a luggin capillary bent tube, which was filled with Cl^- ions solution. The MS surface was prepared by mechanically abrasion with emery paper ranging from 100 to 1000 grade, and washed with acetone. The approximate distance from 1 to 1.5 mm (a constant), between the WE surface and the luggin capillary tip, was maintained to avoid any ohmic loss. All measurements were performed in aerated non-stirred 0.5 M H_2SO_4 solutions with and without BDTT, in different Ct, at 298 K. A CHI 760c (CH Instruments, Inc., USA) device was used for determining I and E, when redox reaction took place. Tafel polarization was measured through WE (MS) E vs. SCE. I vs. E curves (PDP) measurements were carried out at a SR of 1.0 mV/s^{-1}. LPR parameter was measured while GP study was done. All impedance measurements were performed with steady state OCP, using AC amplitude signals, with a peak to peak of 5 mv, through the steady state E, at a range from 100 kHz to 10 mHz. Nyquist and Bode curves were obtained by using these calculations.

T effect

T effect on CR was calculated through WL studies, at 298, 308, 318 and 328 K. MS corrosion E_a with and without BDTT was calculated via Arrhenius eq.

Theoretical investigations (DFT)

The interaction between the MS surface and BDTT and their reactivity were investigated through FMO and Mulliken charge population. DFT of BDTT molecule was performed via 8.0.6 Hyperchem modeling software [26]. To speed up calculations, BDTT was initially optimized via parametrized model 3(PM_3). Semi empirical calculations were done with a starting perimeter of 0.01 $kcal/mol^{-1}$ adjustment, through DFT re-optimization. All observations were completed by selecting 6-311G (d,p) basis set, and exchanging it for B3LYP co-relation function [27-29].

Results and discussion

Ec measurements

PDP and LPR measurements

PDP curves for the WE (MS) in the 0.5 M H_2SO_4 solution without and with BDTT, in different Ct, are represented in Fig. 1, at 298 K. Anodic and cathodic reactions, which took place on the MS electrode surface, were inhibited by BDTT molecule. IE(%) values were determined by Eq. (4).

$$IE\ \% = \frac{I_{Acid} - I_{inh}}{I_{Acid}} X\ 100 \quad (4)$$

where I_{Acid} and I_{inh} are I_{corr} density in the 0.5M H_2SO_4 solution without and with BDTT.

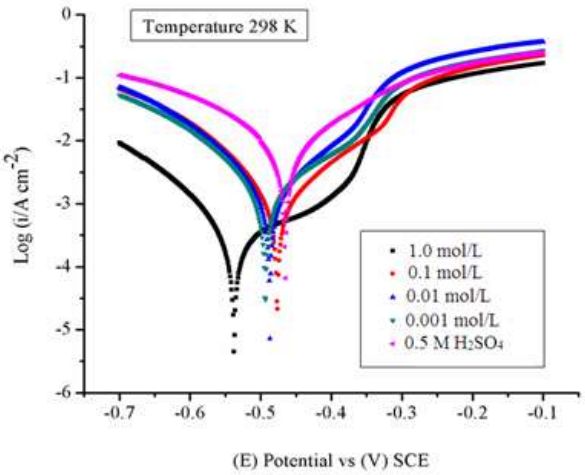

Figure 1: GP curve for MS in a 0.5 M H_2SO_4 medium with different Ct of BDTT, at 298 K.

BDTT effect on anodic reaction was stronger than on the cathodic one. BDTT retarded MS dissolution, which was suggested by the results [30]. Ec corrosion parameters, such as E_{corr}, β_a, β_c and I_{corr}, are given in Table 1. E_{corr} values difference was < 85 mV, which confirms BDTT is a mixed inhibitor type [31]. BDTT adsorption at higher Ct was quite successful, and the CI covered the MS surface almost completely, which revealed its strength. Thus, at higher Ct, BDTT multilayer adsorption took place, which means that the SC of MS was complete, and all corrosion active sites were blocked. However, with lower Ct of CI, SC of MS decreased, and the metal was strongly corroded, due to the decreased IE(%) of BDTT [32, 33].

Table 1: GP and LPR for MS in the 0.5 M H_2SO_4 solution with and without BDTT, in various Ct, at 298 K.

T (K)	Ct (mol/L)	E_{corr} vs. SCE (mV)	- I_{corr} (mA/cm^2)	β_a (mV/dec)	β_c (mV/dec)	IE(%)	R_p	R_p IE(%)
	Blank	465	8.805	60.89	70.59	-	3.8	-
	0.001	493	1.6035	67.30	86.80	81.82	18.7	79.67
298	0.01	487	1.2931	90.29	90.58	85.31	24.4	84.42
	0.1	476	0.8705	80.70	93.80	90.11	35.4	89.26
	1.0	538	0.4067	45.38	91.01	95.38	78.4	95.15

At 298 K, BDTT highest and lowest IE(%) values were 95.38% (1.0 mol/L) and 81.82% (0.001 mol/L), respectively. LPR values revealed that BDTT absorption took place on the MS surface through the development of a non-conducting physical barrier [34]. R_p values rose with higher Ct of BDTT. The increase in SC and BDTT adsorption onto the MS surface, with higher Ct, was confirmed by R_p data (Table 1). Eq. (5) further calculated IE(%).

$$IE\ \% = \frac{(Rp)_{inh} - Rp}{(Rp)_{inh}}\ X\ 100 \qquad (5)$$

where $(R_p)_{inh}$ is R_p value with BDTT.

EIS explanation

EIS gives detailed information about the electrode kinetics and surface characteristics. EIS was performed at 298 K. Nyquist and Bode curves plots for MS in the 0.5 M H_2SO_4 solution without and with BDTT, in different Ct, are shown in Fig. 2a-b.

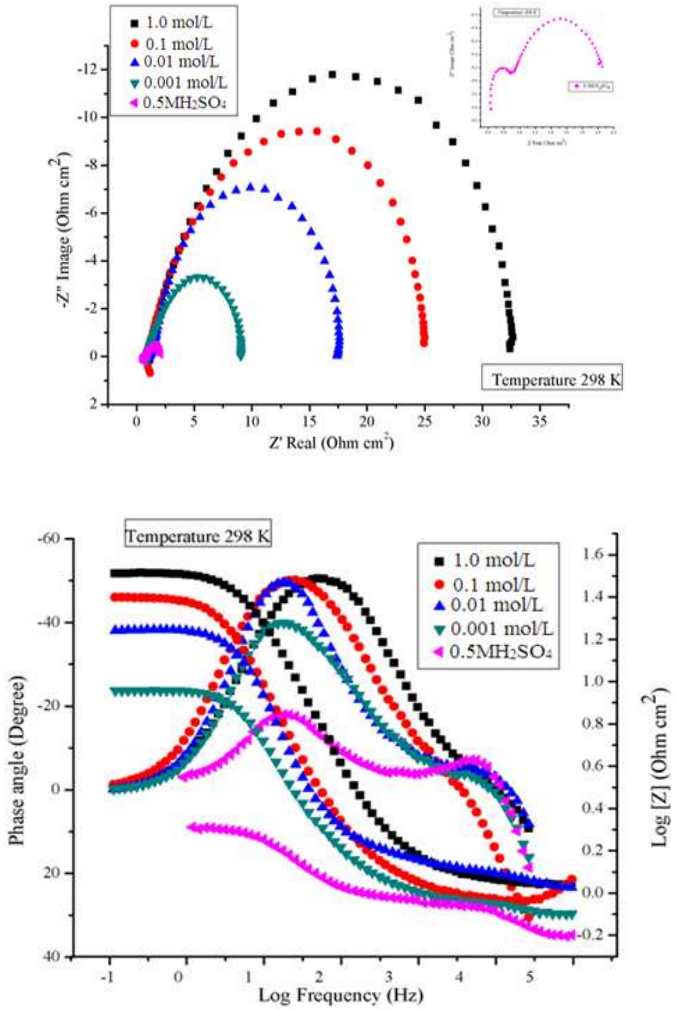

Figure 2 a: Nyquist plots curves for MS in 0.5 M H_2SO_4 without and with BDTT, in different Ct, at 298 K; **b:** Bode plots curves for MS in 0.5 M H_2SO_4 without and with BDTT, in different Ct, at 298 K.

Fig. 2a shows that MS impedance response in H_2SO_4 with BDTT significantly increased. At high-frequencies, the inhibitor system semicircles diameter was noticeably higher than that of the blank solution. This confirms that MS corrosion in H_2SO_4 was inhibited by BDTT.

The various parameters obtained by EIS are shown in Table 2. BDTT molecule IE(%) values were calculated by using Eq. (6).

$$IE\ \% = \frac{(Rct)_{inh} - Rct}{(Rct)_{inh}}\ X\ 100 \qquad (6)$$

where R_{ctinh} is R_{ct} with inhibitor in the H_2SO_4 medium.
In H_2SO_4, the incessantly corroded MS surface became asymmetrical, as reflected on the small phase angle. Thus, BDTT adsorption onto the MS surface decreased, and the phase angle increased, approaching 90° [35]. Fig. 2b capacitive behavior in MS with BDTT is depicted by Bode plot.
The MS/solution interface capacity increased due to BDTT adsorption on it [36]. C_{dl} was calculated by using Eq (7). Table 2 shows that R_{ct} decreased and C_{dl} increased, with higher Ct of BDTT and its larger SC of the MS surface, which improved IE(%) [37].

$$\mathrm{Cdl} = \frac{1}{2\pi R_{ct} F_{max}} \qquad (7)$$

where F_{max} is the maximum frequency through Nyquist plot.
Eq. (8), C_{dl} values decreased towards a constant local dielectric lower value, and the protective layer thickness increased, which enabled BDTT adsorption at the MS/solution interface [38].

$$\mathrm{Cdl\ (capacitance)} = \frac{A\epsilon\varepsilon_\circ}{d} \qquad (8)$$

where A is the electrode surface area, Ɛ and Ɛ^o are the medium dielectric constants and vacuum permittivity, respectively, and d is protective layer thickness. Further, in Table 2, C_{dl} values decreased with higher Ct of BDTT, confirming the rise in the protective layer thickness, which means that d value in Eq (8) increased.
Surface heterogeneity is related to phase shifts that are known n values from Eq. (9).

$$\mathrm{Cdl} = Q(\omega)^{n-1} = Q(2\pi F_{zm-max})^{n-1} \qquad (9)$$

where Q is CPE and ω is part of the impedance spectrum imaginary value, with maximum angular frequency.
Herein, n values were close to one, with higher Ct of BDTT molecule, which enabled the interface to achieve capacitance [39]. BDTT reached IE(%) of 95.44 and 79.51, at 1.0 and 0.001 mol/L respectively, which revealed that it was an effective inhibitor of MS corrosion in H_2SO_4.

Table 2: EIS parameters for MS in a 0.5 M H_2SO_4 solution without and with BDTT, in various Ct, at 298 K.

Ct mol/L	R_s (Ω/cm^2)	Y_0 ($10^{-6}/\Omega^{-1}/cm^{-2}$)	n	R_{ct} (Ω/cm^2)	C_{dl} (Ω/cm^2)	IE(%)
Blank	1.2	158	0.750	1.584	1990	-
0.001	1.0	123	0.795	7.734	492	79.51
0.01	1.1	50	0.801	15.757	263	89.94
0.1	1.2	21	0.825	23.821	146	93.35
1.0	1.1	19	0.845	33.681	129	95.44

WL studies

WL technique provides essential information on CR of MS and IE(%) of BDTT [40]. WL test was carried out on MS coupons (1 x 1 cm) immersed in 0.5 M H_2SO_4,

at different Ct of BDTT, for 24 h, from 298 to 328 K. The graphs plot between CR of MS and Ct of BDTT are shown in Fig. (3).

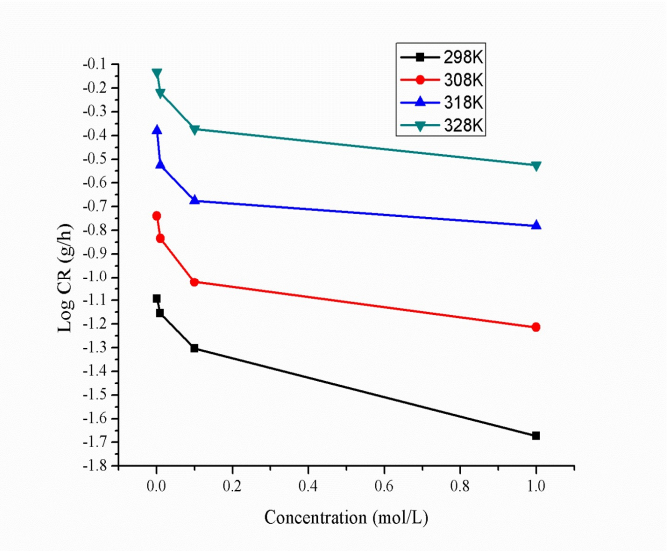

Figure 3: Graph of CR vs. different Ct of BDTT at a T range from 298 to 328 K.

The graphs for IE(%) of BDTT vs. its Ct in the 0.5 M H_2SO_4 solution are shown in Fig 4. CR decreased and IE(%) increased with a rise in Ct of BDTT (Fig. 3 and Table 3), in aggressive environments (Fig. 4). The better properties of the studied inhibitor may be explained through transfer of charge/donation of electrons, because BDTT was adsorbed by the MS surface, reducing its dissolution in H_2SO_4.

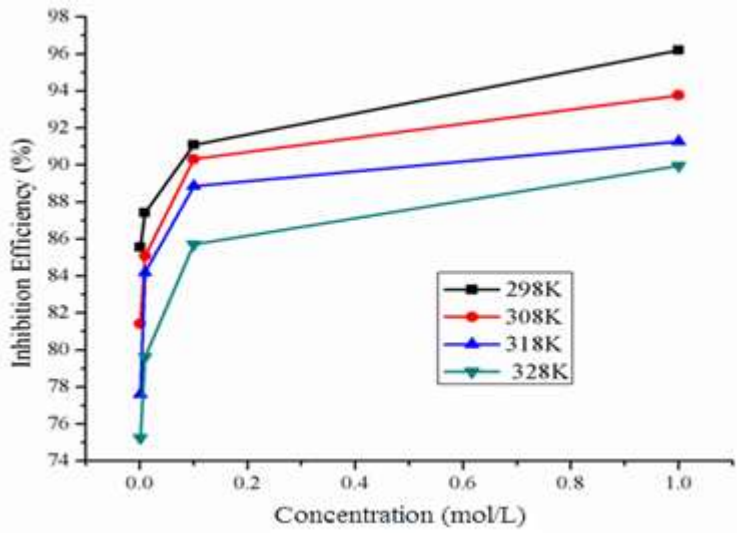

Figure 4: Graph of relationship between IE(%) of BDTT and its Ct.

BDTT adsorption capability is due to its molecules structure, with lone pair heteroatoms, multiple pi bonds and an aromatic system. Herein, the highest and lowest IE(%) of BDTT were 96.19% (1.0 mol/L) and 85.55% (0.001 mol/L), respectively. Fig. 4 and Table 3 show that a rise in T increased CR of MS and decreased IE(%) of BDTT. Therefore, MS dissolution took place, and HER was promoted.

Table 3: WL estimations parameters for MS in 0.5 M H_2SO_4 without and with BDTT, in various Ct, at different T (298-328 K).

T	Ct (mol/L)	CR (gm/h)	IE%	SC (θ)
298 K	blank	0.5571	0	0
	1.0	0.0212	96.19	0.9619
	0.1	0.0497	91.07	0.9107
	0.01	0.0701	87.41	0.8741
	0.001	0.0805	85.55	0.8555
308 K	blank	0.9821	0	0
	1.0	0.0611	93.77	0.9377
	0.1	0.0951	90.31	0.9031
	0.01	0.1465	85.08	0.8508
	0.001	0.1824	81.42	0.8142
318 K	blank	1.8927	0	0
	1.0	0.1652	91.27	0.9127
	0.1	0.2111	88.84	0.8884
	0.01	0.2991	84.19	0.8419
	0.001	0.4165	77.99	0.7799
328 K	blank	2.9682	0	0
	1.0	0.2981	89.95	0.8995
	0.1	0.4243	85.70	0.8570
	0.01	0.6051	79.61	0.7961
	0.001	0.7351	75.24	0.7524

T kinetics (adsorption and activation Td parameters)

Adsorption isotherm

Adsorption isotherms explain the interaction between MS surfaces and BDTT molecules. The water molecules replacement involved the adsorption in the metal/solution interface, via the following process [41, 42]:

$$Org_{(sol)} + nH_2O_{(ads)} \rightarrow Org_{(ads)} + nH_2O_{(sol)} \quad (10)$$

Temkin's, Freundlich's, Frumkin's, Langmuir's, Henry's, Viral's, Damaskin's, Volmer's and Flory-Huggins's adsorption isotherms [40, 41] were tested through the best fit with experimental data. BDTT molecule best adsorption behavior was explained by Langmuir's isotherm [42]. From the determination, R^2 values were equal to one. This adsorption isotherm was depicted by Eq. (11).

$$\frac{C_{inh}}{\theta} = \frac{1}{K_{ads}} + C_{inh} \quad (11)$$

where θ is SC degree and C_{inh} is Ct of BDTT. The relationships between C_{inh}/θ and C_{inh} were linear (Fig. 5), which suggests that BDTT molecule adsorption onto the MS surface obeyed Langmuir's isotherm with every studied T.

$\Delta G°_{ads}$ for BDTT molecule adsorption onto the MS surface was calculated by Eq. (12).

$$\Delta G^{\circ}_{ads} = -2.303\, RT\, [\log(55.5) + logK] \quad (12)$$

From Eq. (12), 55.5 is the Ct of water molecule in the solution. $\Delta G°_{ads}$ values are negative, which means that BDTT molecule adsorption onto the MS surface was a spontaneous process, at all T [45]. Usually, if $\Delta G°_{ads}$ values are nearby -20 kJ/mol^{-1} or less, the adsorption process establishes an electrostatic interaction between the charged metal surface and inhibitor molecules, i.e. "physisorption" [46]. If $\Delta G°_{ads}$ values are around than -40 kj/mol^{-1} or more, the adsorption process occurs via charge transfer or sharing between the inhibitor molecules and the metal surface, and formation of a coordinate bond with the metal, i.e. "chemisorption" [47].

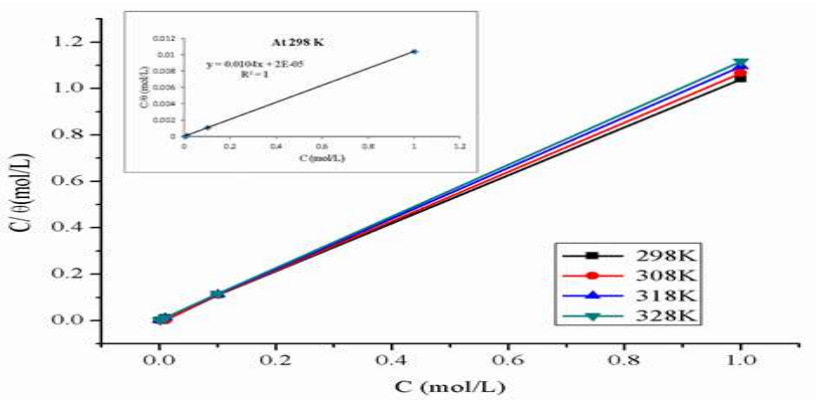

Figure 5: Langmuir's isotherm for BDTT (with various Ct) adsorption onto the MS surface in 0.5 M H_2SO_4, at several T.

In this study, ΔG^0_{ads} values were above 40 kj/mol^{-1} (Table 4), which indicates that BDTT molecule absorption onto the MS surface was chemisorption.

Table 4: Td parameters for BDTT adsorption onto the MS surface in a 0.5 M H_2SO_4 solution, at various T.

T (K)	ln K	R^2	ΔH^0_{ads} (kJ/mol	ΔS^0_{ads} (kJ/mol)	ΔG^0_{ads} (kJ/mol)
298	13.12	1.0			42.44
308	13.12	0.9998	62.12	58.60	44.63
318	11.51	0.9996			41.03
328	10.81	0.9998			40.41

Other Td parameters, such as $\Delta S°_{ads}$ and $\Delta H°_{ads}$ were calculated by Eqs. (13) and (14).

$$\Delta G^{\circ}_{ads} = \Delta H^{\circ}_{ads} - T\Delta S^{\circ}_{ads} \quad (13)$$

$$lnK_{ads} = -\frac{-\Delta H^{\circ}_{ads}}{RT} + \frac{\Delta S^{\circ}_{ads}}{R} - \ln(55.5) \quad (14)$$

The graph plot between ln K_{ads} versus 1/T for BDTT molecule adsorption is shown in Fig. (6).

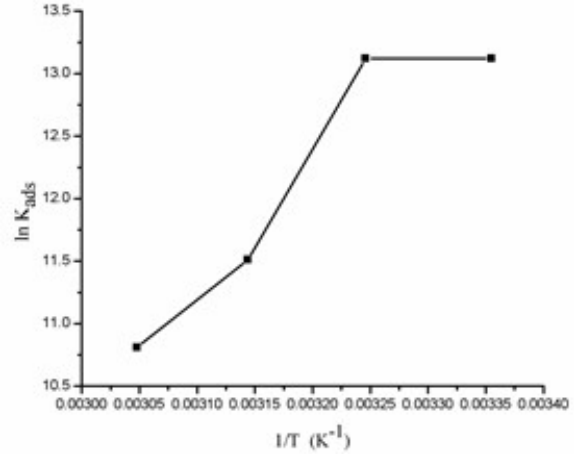

Figure 6: Graph of log K_{ads} vs. 1/T $\Delta G°_{ads}$ for BDTT onto the MS surface.

From eq. (14), a straight line best fit was obtained for $\Delta H°_{ads}$ /R slope and $\Delta S°_{ads}$ /R-ln (55.5) intercept [48].

These Td parameters provide helpful information on the inhibitor molecule adsorption via CI mechanism. When $\Delta H°_{ads} > 0$, the adsorption process is endothermic (chemisorption). When $\Delta H°_{ads} < 0$, the adsorption process is exothermic (physisorption, chemisorption or an involution of both) [46]. Herein, $\Delta H°_{ads}$ and $\Delta S°_{ads}$ values were -61.12 kJ/mol^{-1} and 58.60 J/mol^{-1}/K^{-1}, respectively. Therefore, BDTT adsorption mechanism was a mixture of chemisorption and physisorption [47].

E_a parameters

Further, Td parameters for E_a values were calculated by using Arrhenius graph (Fig. 7), which were obtained from Arrhenius Eq. (15), with and without BDTT molecule, using the slopes for log I_{corr} vs. 1/T (Table 5).

$$\log (I_{corr}) = logA - (\frac{-Ea}{2.30RT}) \quad (15)$$

where A is pre-exponential factor and R is universal gas constant.

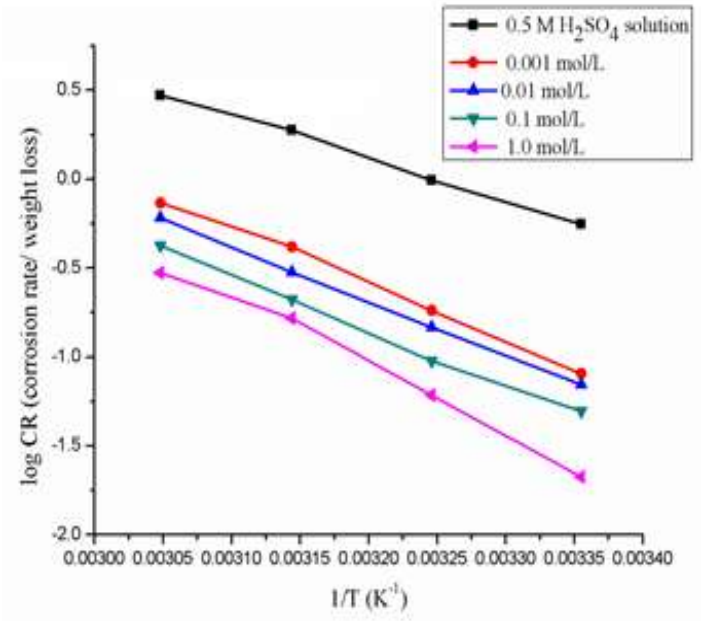

Figure 7: Graph of Arrhenius log (CR of MS) vs. 1/T in a 0.5 M H_2SO_4 solution with various Ct of BDTT.

Table 5: E_a parameters for MS in a 0.5 M H_2SO_4 solution with and without several Ct of BDTT.

Molecule	Ct	E_a (kj/mol)
	Blank	46.27
	0.001	61.51
BDTT	0.01	59.04
	0.1	59.49
	1.0	73.65

MS surface E_a was high, which means that BDTT worked as anti-corrosion catalyst. [48] stated that E_a low values with reduced inhibitor Ct are associated with chemisorption, whereas high E_a values with increased inhibitor Ct correspond to physisorption.

DFT treatment (computational study)

BDTT molecule structures were optimized using DFT hybrid functional as (6-311G B3LYP), which are shown in Figs. 8a- 8c. Quantum chemical parameters are given in Table 6. According to FMO theory, a transition state is developed due to the interaction between HOMO and LUMO [49]. HOMO usually has the ability of donating electrons via the inhibitor molecule. E_{HOMO} high value indicates electron donation to a suitable acceptor molecule with unfilled molecular orbitals of low energy. Increased E_{HOMO} values empower the adsorption by influencing the transportation process [50]. E_{LUMO} represents the capability to accept electrons of the inhibitor molecules. E_{LUMO} low values exhibit high acceptability of inhibitor molecules electrons. BDDT density distributions in FMO are shown in Fig. (8 b) (HOMO) and Fig. 8 c (LUMO). HOMO electron density in BDTT molecule is regularly dispersed close to N and S atoms, which specifies that the molecule has suitable sites for interaction with the MS surface.

LUMO electron density on BDTT dispersed approxim. over the whole inhibitor molecule. So, BDTT molecule was adsorbed on the MS surface, due to π electrons delocalization within the aromatic system, and also to the lone pair electrons in the hetero atoms. BDTT molecule adsorption was strong, due to the delocalized π electrons availability in the ring, and closeness to the MS surface.

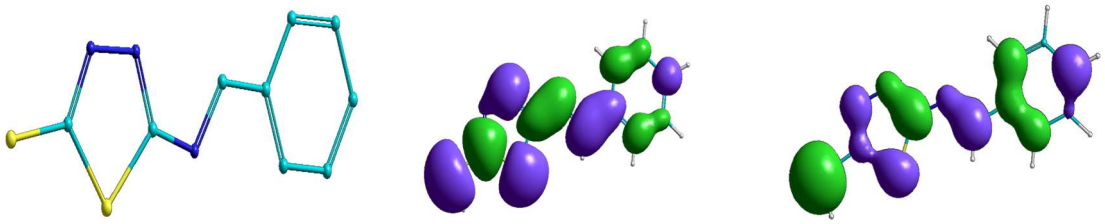

(a) **(b)** **(c)**

Figure 8: BDTT molecule quantum **(a)** optimized structure via DFT; **(b)** HOMO; **(c)** LUMO.

From the DFT analysis of results shown in Table 6, BDTT molecule has high E_{HOMO} and low E_{LUMO} values, and ΔE for the BDTT molecule is given by eq. (16). ΔE value lower than 4.3301 eV means that BDTT molecule has good IE(%). The molecule electronic charge depicts the binding ability of that molecule, via chelating atoms, with the MS surface. The Mulliken charges of BDTT atoms represent the binding ability of that molecule with the MS surface [51]. The chelating or binding ability between the metal surface and the inhibitor molecule depends on the electronic charge of the active or chelating atom. This means that, with higher negative charges, the binding ability is stronger. Table 6 shows other

parameters that were also calculated via Eqs. 16 to 24: ΔN, η, σ, π, $\Delta E_{backdonation}$, (the energy difference between back-donation and electron transfers through the inhibitor molecule) and μ.

$$I = - E_{HOMO} \quad (17)$$

$$A = - E_{LUMO} \quad (16)$$

where I and A are IP and EA, respectively.

$$\Delta E = E_{HOMO} - E_{LUMO} \quad (18)$$

ΔE is high with a hard molecule and high with a soft molecule [52]. BDTT molecular reactivity and stability were evaluated via global η and σ in Eqs. (19) and (20). Chemical η is the resistance to distortion or electrons clouds on atoms, molecules or ions, whereby polarization is almost unaffected by chemical reactions. Herein, BDTT value of η was 2.1650 eV. Generally, global η low value is likely to support greater IE(%) [50]. Normally, adsorption occurs due to electrons transfer through the inhibitor molecule and σ high value [52]. BDTT had a σ value of 0.4618 eV^{-1}, which means it had great IE(%).

$$\eta = \frac{I-A}{2} \quad (19)$$

$$\sigma = \frac{I}{\gamma} \quad (20)$$

χ value describes inhibitor molecules attraction ability. When they have high χ values, their attracting power is stronger, and they have a stronger interaction with the metal surface, so as to accept electrons from it, which enables great IE(%). Herein, χ value calculated via Eq. (21) was 3.9891eV.

$$\chi = \frac{I + A}{2} \quad (21)$$

ΔN was calculated via Eq. (22) , where χ_{Fe} is 7 eV and ηFe equals 0.

$$\Delta N = \frac{(\chi_{Fe} + \chi_{inh})}{2(\eta_{Fe+} \eta_{inh}} \quad (22)$$

Table 6 shows ΔN significance: if ΔN > 0, the electrons transfer occurs towards the metal surface; if ΔN < 0, the electrons transfer occurs from the MS surface onto the inhibitor molecule [52]. As [53] has reported, ΔN < 3.6, which increases IE(%), with the inhibitor molecule rising ability to donate electrons to the metal surface. Herein, ΔN value was 0.6953, which indicates BDTT molecule ability to donate electrons to the MS surface, through the formation of a coordinate bond.

Table 6: DFT parameters via quantum chemical analysis for the inhibitor molecule.

E_{HOMO} (eV)	E_{LUMO} (eV)	ΔE (eV)	Total ener. (kj/mol)	β (eV)	γ (eV)	Σ $(eV)^{-1}$	ΔN	M (Debye)	Π (eV)	$\Delta E_{Back\ donation}$
-6.1542	-1.8241	4.3301	335,471.11	3.9891	2.1650	0.4618	0.6953	3.021	-3.9891	0.5412

Eq. (23) shows that IE(%) of an inhibitor molecule depends upon π [54]. High π values improve the inhibitor molecule ability to release electrons.

$$\pi = \frac{2(\sigma_{Fe})}{-\eta} \quad (23)$$

Eq. (24) calculates electrons charge transfer for donation or back donation [55]. Electronic back-donation occurs through the interaction between the MS surface and the inhibitor molecule. The change in energy is straightly associated with η of BDTT, as shown in Eq. (24), which implies that, when $\eta > 0$ or $\Delta E_{Back\ Donation} < 0$, charge transfer is followed by back-donation via the inhibitor molecule.

$$\Delta E_{backdonation} = \frac{\eta}{4} \quad (24)$$

Herein, $\Delta E_{backdonation}$ and η were 0.5412eV and 2.1650Ev, respectively. These values confirm the molecule ability to act as CI. μ is an additional parameter for the electronic charge distribution throughout a molecule, revealing its structure [54]. No substantial relation between IE(%) and μ values was discovered.

Corrosion mechanism

In this study, BDTT molecule formed a protective layer onto the MS surface in 0.5 M H_2SO_4, during Ec analyses and WL test. BDTT performed successfully as CI for MS in the aggressive medium, at low T, and higher Ct, for a longer IT. BDTT molecule was adsorbed on the MS surface, due to interactions between hetero atoms (N and S) electron pairs, electrons clouds over imine bond and π-electrons clouds delocalized over aromatic rings with the Fe atoms containing empty d-orbitals. BDTT gained protons in the corrosion process, due to its basic character, and reached equilibrium, as Eq. (26) shows, being equivalent to neutral.

$$BDTT + H^+ \leftrightarrow BDTTH^+ \quad (26)$$

In 0.5 M H_2SO_4, due to negative charge, sulfate ions developed an additional charge density on the positively charged MS surface. This means $BDTTH^+$ species had stronger adsorption abilities.

HER follows reactions [56, 57], as depicted in eqs. (27) to (29).

$$Fe + H^+ + e^- \leftrightarrow (FeH)_{ads} \quad (27)$$

$$Fe + (BDTTH^+)_{ads} + e- \rightarrow (Fe.\ BDTTH)_{ads} \quad (28)$$

$$(FeH)_{ads} + (FeH)_{ads} \rightarrow Fe + H_2 \quad (29)$$

H reduction at the cathode into H_2 gas ceased, and $BDTTH^+$ species was competitively adsorbed onto the MS surface.

Conclusions

In the present study, synthesized BDTT behaved as anti-corrosion catalyst for MS substrate in 0.5 M H_2SO_4. The highest observed IE(%) of BDTT (1.0 mol/L) was 95.38%, at 298 K. BDTT adsorption onto the MS surface obeyed Langmuir's

monolayer isotherm. Ec techniques (EIS) associated R_{ct} improvement with higher Ct of BDTT and decreased C_{dl} values. PDP and LPR measurements showed better IE(%) of BDTT with its higher Ct. DFT calculation also supplemented preceding outcomes.

Authors' contributions

Ompal S. Yadav: made the original plan of the research and wrote the manuscript; performed experiments; analyzed and interpreted the results. **Reshu Chaudhary:** performed experiments; validated results; prepared the manuscript. **Ashu Gupta:** validated results; prepared the manuscript.

Acknowledgment

This study was supported by principal Rabi Narayan Kar, Shyamlal College, University of Delhi. All the authors acknowledge the financial support provided from DBT-Star College Scheme. They also thank for the research facilities provided by the Department of Chemistry Shyamlal College and the University Science Instrumentation Centre (USIC), University of Delhi.

Abbreviations

AC: alternating current
AR: analytical research
B3LYP: Becke-3-LeeYang-Parr
BDTT: (E)-5- (benzylideneamino)-1,3,4 thiadiazole-2-thiol (green azo methane)
$C_2H_3N_3S$: 5 amino-1,3,4 thiadiazole- 2- thiol
C_2H_6O: ethanol
C_7H_6O: benzaldehyde
C_{dl}: double layer capacitance
CI: corrosion inhibition/inhibitor
C_{inh}: inhibitor concentration
CPE: constant phase element
CR: corrosion rate
Ct: concentration
DFT: density functional theory
E: potential
E_a: activation energy
Ec: electrochemical
E_{corr}: corrosion potential
E_{HOMO}: energy of the highest occupied molecular orbital
EIS: electrochemical impedance spectroscopy
E_{LUMO}: energy of the lowest occupied molecular orbital
FMO: frontier molecular orbital
GP: galvanostatic polarization
H_2SO_4: sulfuric acid
HER: hydrogen evolution reaction
HOMO: highest occupied molecular orbital
I: current
I_{corr}: corrosion current

IE(%): inhibition efficiency
IP: ionization potential
IT: immersion time
K_{ads}: constant of adsorptive equilibrium
LPR: linear polarization resistance
LUMO: lowest unoccupied molecular orbital
MS: mild steel
OCP: open circuit potential
PDP: potentiodynamic polarization
R^2: regression coefficient
R_{ct}: charge transfer resistance
R_p: polarization resistance
SC: surface coverage (θ)
SR: scan rate
T: temperature
Td: thermodynamic
TLC: thin-layer chromatography
WL: weight loss

Symbols definition
β_a: anodic Tafel slope
β_c: cathodic Tafel slope
ΔE: energy gap
$\Delta G°_{ads}$: standard free energy of adsorption
$\Delta H°_{ads}$: standard enthalpy
ΔN: fraction of transferred electrons
$\Delta S°_{ads}$: standard entropy
η: absolute hardness
μ: dipole moment
σ: softness index
χ: absolute electronegativity
π: chemical potential

References

1. Leçe HD, Emregül KC, Atakol O. Difference in the inhibitive effect of some Schiff base compounds containing oxygen, nitrogen and sulfur donors. Corros Sci. 2008;50(5):1460-1468. https://doi.org/10.1016/j.corsci.2008.01.014
2. Sahin M, Gece G, Karcı F, Bilgiç S. Experimental and theoretical study of the effect of some heterocyclic compounds on the corrosion of low carbon steel in 3.5% NaCl medium. J Appl Electrochem. 2008;38:809-815. https://doi.org/10.1007/s10800-008-9517-3
3. Aljourani J, Raeissi K, Golozar MA. Benzimidazole and its derivatives as corrosion inhibitors for mild steel in 1M HCl solution. Corros Sci. 2009;51:1836-1843. https://doi.org/10.1016/j.corsci.2009.05.011
4. Zheludkevich ML, Yasakau KA, Poznyak SK et al. Triazole and thiazole derivatives as corrosion inhibitors forAA2024 aluminum alloy. Corros Sci. 2005;47(12):3368-3383. https://doi.org/10.1016/j.corsci.2005.05.040

5. Obot IB, Obi-Egbedi NO, Umoren SA. The synergistic inhibitive effect and some quantum chemical parameters of 2,3-diaminonaphthalene and iodide ions on the hydrochloric acid corrosion of aluminium. Corros Sci. 2009;51(2):276-282.
6. Hosseini MG, Ehteshamzadeh M, Shahrabi T. Protection of mild steel corrosion with Schiff bases in 0.5 M H_2SO_4 solution. Electrochim Acta. 2007;52(11):3680-3685.
7. Villamizar W, Casales M, Gonzalez-Rodriguez JG et al. CO_2 corrosion inhibition by hydroxyethyl, aminoethyl and amidoethyl imidazolines in water–oil mixtures. J Solid State Electrochem. 2007;11(5):619-629.
8. Sastri VS. Green Corrosion Inhibitors: Theory and Practice, John Wiley & Sons Inc Hoboken New Jersey. 2011.
9. Manahan SE. Environmental Chemistry. CRC Press New York USA. 1994.
10. Yadav DK and Quraishi MA. Electrochemical investigation of Substituted Pyranopyrazoles Adsorption on Mild Steel in Acid Solution. Ind Eng Chem Res. 2012;51(24):8194-8210.
11. Khadom AA, Musa AY, Kadhum AH et al. Adsorption Kinetics of 4-Amino-5-Phenyl-4H-1, 2, 4- Triazole-3-Thiol on mild steel surface. Port Electrochim Acta. 2010;28(4):22230. https://doi.org/10.4152/pea.201004221
12. Abuelela AM, Bedair MA, Zoghaib WM et al. Molecular structure and MS/HCl corrosion inhibition of 4, 5 Dicyanoimidazole: vibrational, electrochemical and quantum mechanical calculations. J Mol Struct. 2021;1230:article id 129647. https://doi.org/10.1016/ j.molstruc.2020.129647
13. Al-Amiery A, Shaker L, Kadhum A et al. Corrosion inhibition in strong acid environment by 4-((5,5-dimethyl-3-oxocyclohex-1-en-1yl)amino)benzenesulfonamide. Tribology indust. 2020;42(1). https://doi.org/10.24874/ti.2020.42.01.09
14. Caldona EB, Zhang M, Liang G et al. Corrosion inhibition of mild steel in acidic medium by simple azole-based aromatic compounds. J Electroanalyt Chem. 2021;880:114858.
15. Chaouiki A, Chafiq M, Rbaa M et al. Comprehensive assessment of corrosion inhibition mechanisms of novel benzimidazole compounds for mild steel in HCl: an experimental and theoretical investigation. J Mol Liq. 2020;320:114383.
16. Lgaz H, Saha SK, Chaouiki A et al. Exploring the potential role of pyrazoline derivatives in corrosion inhibition of mild steel in hydrochloric acid solution: insights from experimental and computational studies. Construct Build Mat. 2020;233:117320.
17. Muthamma K, Kumari P, Lavanya M et al. Corrosion inhibition of mild steel in acidic media by N-[(3, 4- dimethoxyphenyl) methyleneamino]-4-hydroxy-benzamide. J Bio Tribo-Corros. 2021;7(1):1e19. https:// doi.org/10.1007/s40735-020-00439-7
18. Shetty P. Schiff bases: an overview of their corrosion inhibition activity in acid media against mild steel. Chem Eng Commun. 2020;207(7):985e1029. https://doi.org/10.1080/ 00986445.2019.1630387

19. Popova A, Christov M, Zwetanova A. Effect of the molecular structure on the inhibitor properties of azoles on mild steel corrosion in 1 M hydrochloric acid. Corros Sci. 2007;49(5):2131-2143.
20. Issaadi S, Douadi T, Zouaoui A et al. Novel thiophene symmetrical Schiff base compounds as corrosion inhibitor for mild steel in acidic media. Corros Sci. 2011;53(4):1484-1488.
21. Ansari KR, Quraishi MA, Singh A. Schiff's base of pyridyl substituted triazoles as new and effective corrosion inhibitors for mild steel in hydrochloric acid solution. Corros Sci. 2014;79:5-15.
22. Kajal A, Bala S, Kamboj S et al. Schiff Bases: A Versatile Pharmacophore. 2013;ArticleID893512;pages14.
23. Umoren SA, Obot IB, Madhankumar A et al. Performance evaluation of pectin as ecofriendly corrosion inhibitor for X60 pipeline steel in acid medium: experimental and theoretical approaches. Carbohydr Polym. 2015;124; 280e291. https://doi.org/10.1016/j.carbpol.2015.02.036
24. Mobin M, Aslam R, Aslam J. Non-toxic biodegradable cationic Gemini surfactants as novel corrosion inhibitor for mild steel in hydrochloric acid medium and synergistic effect of sodium salicylate: experimental and theoretical approach. Mater Chem Phys.2017;191:151e167.
25. Kumar S, Kalia V, Goyal M et al. Newly synthesized oxadiazole derivatives as corrosion inhibitors for mild steel in acidic medium: Experimental and theoretical approaches. J Mol Liq. 2022;357:119077.
26. HyperChem (TM) Professional 8.0.6, Hypercube Inc. Gainesville, FL, USA, 2007.
27. Stewart JJP. Optimization of parameters for semi-empirical methods I. Method. J Compu. Chem. 1989;10(2): 209-220.
28. Becke AD. Density-functional thermochemistry. III. The role of exact exchange. J Chem Phys. 1993;98:5648. https://doi.org/10.1063/1.464913
29. Lee C, Yang WT, Parr RG. Development of the Colle-Salvetti Correlation-Energy Formula into a Functional of the Electron Density. Phys Rev B. 1988;37:785-789.
30. Hegazy MA, Hasan AM, Emara MM et al. Evaluating four synthesized Schiff bases as corrosion inhibitors on the carbon steel in 1 M hydrochloric acid. Corros Sci. 2012;65:67-76.
31. Xianghong Li, Shuduan D, Hui F. Triazolyl blue tetrazolium bromide as a novel corrosion inhibitor for steel in HCl and H_2SO_4 solutions. Corros Sci. 2011;53:302-309.
32. Saleh MM, Atia AA. Effects of structure of the ionic head of cationic surfactant on its inhibition of acid corrosion of mild steel. J Appl Electrochem. 2006;36:899-905.
33. Ferreira ES, Giacomelli C, Giacomelli FC et al. Evaluation of the inhibitor effect of l-ascorbic acid on the corrosion of mild steel. Mat Chem Phys. 2004;83(1):129-134.
34. Babic-Samardzija K, Lupu C, Hackerman NE et al. Inhibitive properties and surface morphology of a group of heterocyclic diazoles as inhibitors for acidic iron corrosion. Langmuir. 2005;21:12187-12196.

35. Deslouis C, Tribollet B, Mengoli G et al. Electrochemical behavior of copper in neutral aerated chloride solution. Steady-state investigation. J Appl Electrochem.1988;18:374-383.
36. Oguzie EE, Lia Y, Wang FH. Effect of 2-amino-3-mercaptopropanoic acid (cysteine) on the corrosion behaviour of low carbon steel in sulphuric acid. Electrochim Acta. 2007;53(2):909-914.
37. Singh AK, Quraishi MA. Inhibiting Effects of 5-Substituted at in-Based Mannich Bases on the Corrosion of Mild Steel in Hydrochloric Acid Solution. J Appl Electrochem. 2010;40:1293-1306.
38. Gerengi H, Sahin HI. *Schinopsis lore*ntzii Extract as a Green Corrosion Inhibitor for Low Carbon Steel in 1 M HCl Solution. Ind Eng Chem Res. 2012;51(2):780-787.
39. Singh SK, Tambe SP, Gunasekaran G, Raja VS, Kumar D. Electrochemical impedance study of thermally sprayable polyethylene coatings. Corros Sci. 2009;51(3):595-601.
40. Bentiss F, Traisnel M, Gengembre L et al. New triazole derivative as inhibitor of the acid corrosion of mild steel: Electrochemical studies, weight loss determination, SEM and XPS. Appl Surf Sci.1999;152:237-249.
41. Gabrielli C. Identification of Electrochemical Processes by Frequency Response Analysis Solartron Franborough UK. 1980 62.
42. Kalman E, Varhegi B, Bako I et al. Corrosion inhibition by 1-Hydroxy-ethane-1, 1-diphosphonic acid an electrochemical impedance spectroscopy study. J Electrochem Soc. 1994;141:3357-3360.
43. Bellman C, Stamm M. Polymer Surfaces and Interfaces. Springer Berlin. 2008.
44. Mu G, Li X, Qu Q et al. Molybdate and tungstate as corrosion inhibitors for cold rolling steel in hydrochloric acid solution. Corros Sci. 2006;48:445-459.
45. Oguzie EE, Unaegbu C, Ogukwe CN et al. Inhibition of mild steel corrosion in sulphuric acid using indigo dye and synergistic halide additives. Mat Chem Phys. 2004;84:363-368.
46. Oguzie EE. Corrosion inhibitive effect and adsorption behaviour of *Hibiscus sabdariffa* extract on mild steel in acidic media. Port Electrochim Acta. 2008;26(3):303-314.
47. Oguzie EE, Enenebeaku CK, Akalezi CO et al. Adsorption and corrosion-inhibiting effect of *Dacryodis edulis* extract on low-carbon-steel corrosion in acidic media. 2010;349(1):283-292.
48. Marsh J. Advanced Organic Chemistry, third ed. Wiley Eastern. New Delhi, 1988.
49. Fukui K. Theory of Orientation and Stereo selection, Springer-Verlag, New York. 1975.
50. Gece G. The use of quantum chemical methods in corrosion inhibitor studies. Corros Sci. 2008;50:2981-2992.
51. Murrell JN, Kettle SF, Tedder JM. The Chemical Bond, John Wiley & Sons. Chichester;1985.
52. Reed AE, Curtiss LA and Weinhold F. Intermolecular Interactions from a Natural Bond Orbital, Donor-Acceptor Viewpoint. Chem Rev.1988;88:899-926.

53. Pearson RG. Absolute Electronegativity and Hardness: Application to Inorganic Chemistry. Inorgan Chem.1988;27:734-740.
54. Yadav M, Behera D, Kumar S et al. Experimental and quantum chemical studies on corrosion inhibition performance of thiazolidinedione derivatives for mild steel in hydrochloric acid solution. Chem Eng. Commun. 2015;202(3):303-315.
55. Gómez B, Likhanova NV, Domínguez-Aguilar MA et al. Quantum chemical study of the inhibitive properties of 2-pyridyl-azoles. J Phys Chem B. 2006;110:8928-8934.
56. Yadav DK, Quraishi MA, Maiti B. Inhibition effect of some benzylidenes on mild steel in 1 M HCl: an experimental and theoretical correlation. Corros Sci. 2012;55:254-266.
57. Okafor P, Ikpi CME, Uwah IE et al. Inhibitory Action of *Phyllanthus amarus* Extracts on the Corrosion of Mild Steel in Acidic Media. Corros Sci. 2008;50(8):2310-2317.